# AERODYNAMICS AND AEROACOUSTICS INVESTIGATION OF A LOW SPEED SUBSONIC JET OPERATING AT MACH 0.25

Pedro Ricardo Correa Souza, Anderson Ramos Proença and Odenir de Almeida
*Faculty of Mechanical Engineering, Federal University of Uberlândia, Uberlândia, MG, 38408-100*

*and*

Rodney Harold Self
*Institute of Sound and Vibration Research,University of Southampton, Southampton, Hampshire, SO171BJ*

**ABSTRACT**

**Low and high speed subsonic jets have been studied in the last 50 years mainly due its large application in industry, such as the discharge of turbojets and turbofan engines. The purpose of this work is to investigate the aerodynamics and the acoustic noise generated by a single stream jet flow operating at low Mach number 0.25 and Reynolds number of $2{,}1 \times 10^5$. The main focus is the flow and acoustics characterization of this low speed jet by appling different experimental techniques for evaluating the velocity field via measurements with pitot tube and hot-wire anemometry and farfield noise acquisition by free field microphones. In order to verify the validity of aeroacoustics prediction for such low speed jet, a Computational Fluid Dynamics by means of RANS simulations via k-ω SST model have been employed coupled with a statistically low-cost Lighthill-Ray-Tracing method in order to numerically predict the acoustic noise spectrum. Sound pressure level as a function of frequency is contructed from the experiments and compared with the noise calculations from the acoustic modeling. The numerical results for the acoustic and flow fields were well compared with the experimental data, showing that this low-cost flow-acoustic methodology can be used to predict acoustic noise of subsonic jet flows, even at low speeds.**

## 1. Introduction

The noise produced by an aircraft has been one of the most important subjects in last decades for the industry and academic research. It is well known that the noise is generated by different components and by the interaction of external flow and the aircraft parts. According to the aircraft performance, during each phase of flight, one region or equipment should contribute more or less to the "total noise" [1]. In other words, the

aircraft on the ground, while taxing, on run-up from the jet exhaust, during the take-off, underneath to departure and arrival paths, over-flying while in route and landing, produces different noise signatures not only in terms of amplitude but also in its composition – Figure 1.

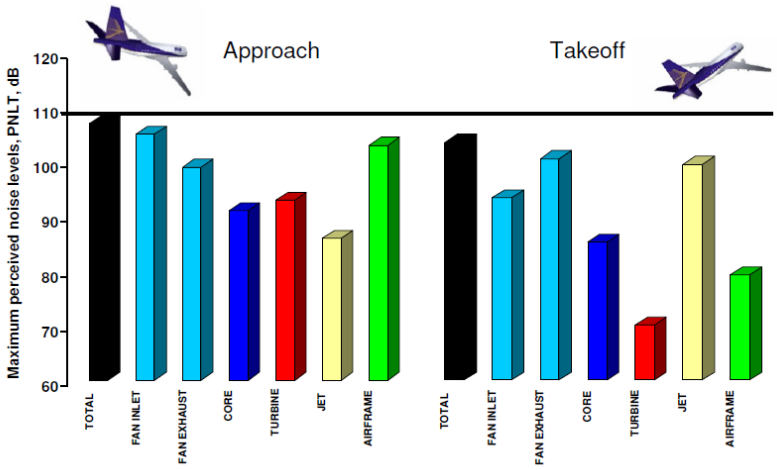


Figure 1. Noise components breakdown at take-off and approach (Almeida, 2009).

According to Fig.1, aircraft have various noise sources being the engines one of the major contributors to the total noise. At take-off and climb, the fan exhaust and jet are the mainly responsible for the noise levels of an aircraft. During the approach the engine noise is also considerable. Although high bypass ratio turbofans engines have experienced advanced modifications and improvements in the last few years, fan noise and jet noise still play the most important role in terms of noise generation [2].

Driven by new noise regulations (FAR) Part 36 [3] and the need to be environmental less impactant, aeronautical industry and academic research centers have invested efforts for understanding and proposing new techniques and ideas to reduce engine and airframe noise. This subject has undoubtedly proved to be quite important in modern aeronautical area and is the main motivation of this work.

The different ways to study engine/airframe noise goes from several experimental techniques up to modern numerical models applied for real articles (engines) or scaled prototypes to be tested in laboratory. Experiments often become prohibited for real scale since the costs involved are too high, leading directly to experiments with reduced model (scaled models) where knowledge about the problem phenomenology, laws of similarity and practical equipments is really useful.

On the other hand, the numerical approach is at least splitted in three main branches, when considering Computational Fluid Dynamics (CFD): Direct Numerical Simulation (DNS) solving all the motion scales of the flow; Subgrid Scale (SGS) modeling where LES (Large Eddy Simulation) is one of the examples, solving

partially the flow scales; and the hybrid or RANS (Reynolds Averaged Navier-Stokes) based methods, including the flow and acoustics analogies and empirical models, solving the main characteristics of the flow.

Experimental research of free jets has been reported for at least one century. From early work of Trupel [4] passing by Abramovich [5], Towsend [6], Lilley [7], Lau and Tester [8] among many others, currently hot-wire, Particle Image Velocimetry (PIV) and modern Laser Doppler (LD) applications have important role in turbulent jet measurements, including the case of jet noise. Measurements made in a low speed air jet (Mach = 0.18) with associated cross-spectra and spectral length scales of the axial and lateral velocity components were performed by Harper-Bourne [9] and enhanced by Morris and Zaman [10], providing a more complete picture of the relevant turbulent statistics, including a wider range of reference points in the jet through cross spectra and cross correlations, second and fourth order statistics and also comparisons with a RANS prediction method. Non-intrusive techniques have been employed by Mielke et al. [11] to measure velocity, density, temperature and turbulence velocity fluctuations in sparsely seeded, high-speed gas flows, used to make measurements in a 25.4 mm diameter free jet at subsonic and supersonic flow conditions.

Bridges et al. [12] used PIV to calculate turbulence quantities in nozzle flows from instantaneous 2D velocity maps. Other published works are related to comparison between experimental and numerical results of free turbulent jets. Ghahremanian and Moshfegh [13] presented numerical results of 3D modeling of an isothermal, free jet with four different RANS turbulence models which were validated against hot-wire anemometry data. The comparison showed and excellent agreement between experimental and numerical results.

Other works are seen in literature showing numerical results validated against proper data or results from others – Freund [14], Stromberg et al. [15] of a simple round jet flow and acoustics. More specific analysis, including the use of chevrons, can be seen in the works of Xia et al. [16], Birch et al. [17] and Engel [18] among others.

In this work, a sequential and comprehensive study about the physics of a subsonic free stream jet is proposed by performing controlled experiments for the evaluation of the flow and acoustics fields, through the use of multiprobe Pitot tube, hot-wire anemometer and farfiel acoustic measurements. A complementary numerical analysis was adopted by a hybrid approach based on RANS modeling coupled with a noise prediction method called Lighthill-Ray-Tracing (LRT) – Silva [19], for fluid flow calculations and the prediction of the sound sources in the flow and its propagation to an observer in the far-field, respectively.

By considering such path, the main contribution of this work was to characterize the flow of a low-speed subsonic jet (Mach = 0.25) by means of experimental measurements and to use such data to validate a low-cost hybrid RANS-based method coupled with the LRT method for predicting the far-field noise and its directivity using the fluid flow properties calculated with the RANS technique as input. The experimental data was used as an original benchmark for the numerical prediction tools, which have constituted a low-cost flow-acoustic methodology for being used at industry. The agreement between the numerical solution and experimental data is very good, showing that this approach can be used to predict acoustic noise of subsonic jet flows, even at low speeds.

## 2. Experimental Measurements

The experimental part of this research was carried out in the Doak Laboratory, a Rolls Royce UTC (University Technologic Center) facility located at ISVR (Institute of Sound and Vibration Research) at University of Souhthampton, United Kingdom. A general description and information about this small scale test facility, will be given in the sequence.

The ISVR's Doak laboratory is a 15m x 7 x 5m anechoic chamber fully anechoic down to 400 Hz. The four walls, ceiling and the floor are covered with wedge type absorbent material. A non-forced exhaust system is composed by a rectangular collector section allowing the air flow to pass through into a small secondary acoustic chamber – Figure 2.

Figure 2. Internal view of the Doak Laboratory – ISVR (after Proença [20]).

The air flow is fed from two high pressure compressed air (20 bar) from two storage tanks and the range of velocity available for testing is from Mach 0.2 up to 1. At these conditions, single jet measurements can be

performed on flow regimes characteristic of civil aircrafts. For jet noise measurements, both polar and a transversable azimuthal array of microphones can be used to give a complete three-dimensional sound field.

### 2.1 Test Article – Convergent Nozzle

The test article used in this work was a 38.1 mm exit-diameter, convergent, conical nozzle used for most of the tests done at the Doak Laboratory. This nozzle was selected because its aerodynamic and acoustic characteristics were well-documented in the Noise Test Facility (NTF) at QinetiQ [21], Farnborough, UK.

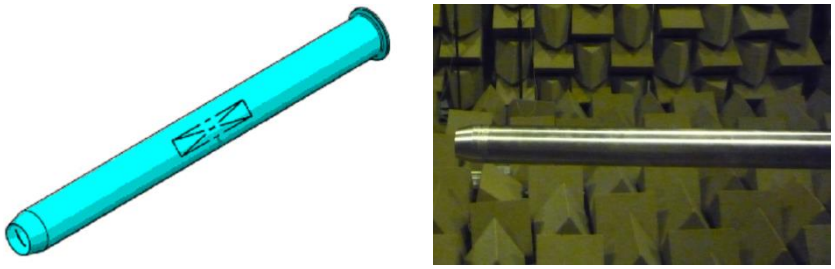

Figure 3. Sketch and picture of 38 mm diameter - reference nozzle, ISVR.

The subsonic jet was operated from the nozzle at isothermal condition running at Mach number of 0.25. In order to run aerodynamics measurements with Pitot tube and hot-wire anemometer, a traverse system was placed inside the anechoic room – Figure 4.

Figure 4. General view of Doak Laboratory with traverse system to hot-wire anemometer and pitot tube measurements – Proença [20].

### 2.2 Acoustic Noise Measurements

Acoustic data is acquired using GRAS Type 40BF microphones, with a frequency range of 10 Hz to 100 kHz and dynamic range of 40 dB to 174 dB (reference 20 µPa), and digitized using a National Instruments NI PCI-4472 acquisition card with a 102.4kHz sample rate, and 24-bit resolution.

The acoustic measurements were performed only to the far-field. Six different observer angles 40°, 50°, 60°, 75°, 90° e 110° were applied to acquire the noise signature. Measurements of Overall Sound Pressure Level (OASPL) are achieved by numerically integrating the narrowband spectra with respect to frequency using a trapezium rule method across the entire range of narrowband frequencies. The narrowband data may also be transformed into one-third octave band spectra using idealised third-octave filters consistent with ANSI S1.1-1986.

### 2.3 Aerodynamics Measurements

The measurements of the mean flow velocity profiles were performed using a Pitot tube, while the hot-wire anemometer is used for mean flow and turbulence intensity measurements – Figure 5.

Figure 5. Pitot tubes and single hot-wire sensors – Proença [20].

The Pitot tube was used to measure mean flow velocity profiles and the spreading of the jet. Furthermore, it was used as a reference velocity measurement to calibrate the hot-wire sensors.

Hot-wire anemometry is the main measuring system applied in this work. Single hot-wire anemometers are the most common sensors applied in flow measurements, for several reasons: reduced size, price relatively low, high frequency response, simple to use. One of the limitations is that it has to be used for low turbulence intensities (up to 10%), which is fine for Mach 0.25 free jets. The velocity distributions were acquired along the jet axis to different radial positions and the workspace of mean velocity profile experiments is demonstrated in the Fig. 6. The center of the nozzle is located at origin x,y = (0,0), where ‘x’ is the jet axis and ‘y’ represents the radial variation. The red dots symbolize where the data were acquired. Only for single hot-wire probes, just the points inside the blue rectangle were acquired. Thus, for the Mach number analyzed, 963 points were recorded to Pitot tube and triple hot-film measurements, whilst 583 to single hot-wire. Additional information for the experimental part of this work can be found in the work of Proença [20].

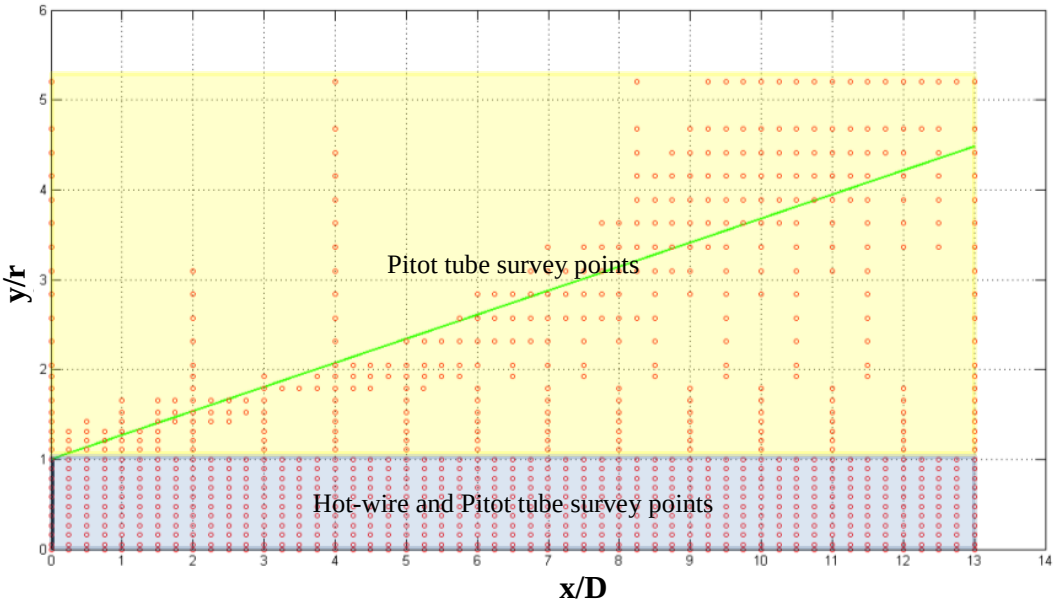


Figure 6. Acquisition points along the region of the jet for aerodynamic measurements – Proença [20].

## 3. Numerical Modeling

This section is concerned with the mathematical modeling used for the fluid flow and acoustic simulations. The aerodynamics simulations were conducted with the well-known CFD++ commercial code [22] and the acoustic predictions were obtained using the LRT method [19].

### 3.1 Aerodynamics Simulation

A Reynolds Averaged Navier-Stokes (RANS) approach is used in this work. The compressible steady-state equations of motion were solved in a tridimensional domain.

The equation system that describes the problem is composed by the continuity, Navier-Stokes and energy equations. Upon using RANS, the term $\overline{\rho u_i'' u_j''}$ that involves the mean of density and velocity fluctuations, appear and the k-ω SST turbulence model is used for closure. This model solves transport equations for turbulent kinetic energy (k) and specific turbulence dissipation rate (ω), using the equations presented below:

$$\overline{\rho u_i'' u_j''} = \frac{2}{3}\delta_{ij}\overline{\rho}k - \mu_t\overline{S_{ij}}; \tag{1}$$

where $\mu_t$ is turbulent viscosity (Eq. 2) and $S_{ij}$ is given by Eq. 3.

$$\frac{\mu_t}{\overline{\rho}} = \nu_t = \frac{a_1 k}{\max\{a_1\omega, SF_2\}} \quad , \quad S = \sqrt{\frac{2\overline{S_{ij}}\,\overline{S_{ij}}}{\beta^*}} \tag{2}$$

$$\overline{S_{ij}} = \left(\frac{\partial\overline{u_i}}{\partial x_j} + \frac{\partial\overline{u_j}}{\partial x_i} - \frac{2}{3}\frac{\partial\overline{u_k}}{\partial x_k}\delta_{ij}\right) \tag{3}$$

The transport equation for turbulence kinetic energy and specific turbulence dissipation rate are:

$$\frac{\partial(\overline{\rho}k)}{\partial t}+\frac{\partial}{\partial x_j}\left(\overline{\rho}\widetilde{u_j}k\right)=\frac{\partial}{\partial x_j}\left[\left(\mu+\sigma_k\mu_t\right)\frac{\partial k}{\partial x_j}\right]+\widetilde{P_k}-\beta^*\overline{\rho}k\omega \quad (4)$$

$$\frac{\partial(\overline{\rho}\omega)}{\partial t}+\frac{\partial}{\partial x_j}\left(\overline{\rho}\widetilde{u_j}\omega\right)=\frac{\partial}{\partial x_j}\left[\left(\mu+\sigma_\omega\mu_t\right)\frac{\partial\omega}{\partial x_j}\right]+\frac{\gamma}{\nu_t}P_k-\beta\overline{\rho}\omega^2+2(1-F_1)\overline{\rho}\sigma_{\omega2}\frac{1}{\omega}\frac{\partial k}{\partial x_j}\frac{\partial\omega}{\partial x_j} \quad (5)$$

More details about functions like $P_k$, $\widetilde{P_k}$, $F_1$, $F_2$ and $CD_{k\omega}$ can be found in [23] work. This model like any other, brings a large number of empirical constants. Except for constants like $\beta^*$and $\kappa$, all the others have to obey Eq. 6, and the values used for them in this study are listed in table 1.

$$\phi=\phi_1F_1+\phi_2(1-F_1) \quad (6)$$

where $\phi$ is a constant.

Table 1. Constants used in k-ω SST model.

| $\sigma_{k1}$ | $\sigma_{k2}$ | $\sigma_{\omega1}$ | $\sigma_{\omega2}$ | $\beta_1$ | $\beta_2$ |
|---|---|---|---|---|---|
| 0.85 | 1.0 | 0.5 | 0.856 | 0.075 | 0.0828 |

| $\gamma_1$ | $\gamma_2$ | $a_1$ | $a_2$ | $\beta^*$ | $\kappa$ |
|---|---|---|---|---|---|
| 0.553 | 0.44 | 5/9 | 0.44 | 0.09 | 0.41 |

Several tests where made previously in order to find the best turbulence model for this problem, although those test won't be shown here as this is not the aim of the article.

The governing equations closed with the k-ω SST model, were solved with a second order accuracy through a Finite Volume formulation. As the jet flow is at Mach lower then 0.3, a preconditioning approach was necessary to stabilize the solution. The final result was obtained when the residual dropped 5 orders of magnitude.

### 3.2 Aeroacoustics Prediction

The sound pressure levels generated by the jet are calculated by the Lighthill Ray-Tracing method (LRT) [19], using the mean flow field characteristics previously calculated by the CFD code. An external Fortran code was implemented in order to receive the CFD input data as u, c, T, ρ, k, ω and to compute the sources generation by discretizing the jet by virtual sound sources further propagated to the farfield by the Ray-Tracing method.

In fact, this method uses the standard Lighthill equations for noise calculations coupled to the Ray-Tracing methodology [24] in order to account for the refractions of sound waves due to velocity gradients present in the

flow field. Thus resulting in a better modeling of the sound propagations than the other well-known RANS-based acoustic methods like the MGBK [25].

According to Jordam and Gervais [26] the acoustic field generated by a jet flow is:

$$p(\vec{y},\theta) = A\, I_{ijkl}\, dir(ijkl) \tag{7}$$

where A is given by Eq. 8, the fourth-order autocorrelation function for a unit volume of turbulence $I_{ijkl}$ and the source directional patterns $dir(ijkl)$ can be calculated by Eq. 9 and 10.

$$A = \frac{\overline{\rho}}{16\pi^2 c^2 R^2 [1-M_c \cos(\theta)]^5} \tag{8}$$

$$I_{ijkl} = \int \frac{\partial^4 \left(\overline{v_i v_j v_k v_l}\right)}{\partial \tau^4} d^3\vec{r} \tag{9}$$

$$dir(ijkl) = \frac{1}{2\pi}\int_0^{2\pi} \left(\frac{x_i x_j x_k x_l}{x^4}\right) d\varphi \tag{10}$$

Using the coordinate system from Fig. 7 and integrating it, it possible to obtain Eq. 11 and 12:

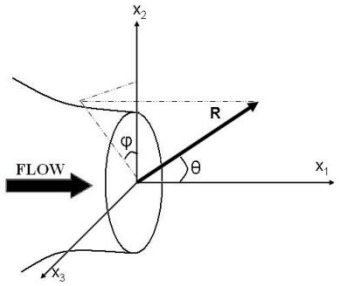

Figure 7. Coordinate system used for the integrations [19].

$$p(\vec{y},\theta) = A(\cos^4\theta)I_{1111} + \frac{6}{8}A(\sin^4\theta)C_1 I_{1111} + 2A(\cos^2\theta\sin^2\theta)C_2 I_{1111} + 4A(\sin^4\theta)C_3 I_{1111} + \\ + 4A(\cos^2\theta\sin^2\theta)C_4 I_{1111} + 2A(\sin^4\theta)C_5 I_{1111} \tag{11}$$

$$I_{1111}(\Omega) = \left[\frac{\sqrt{\pi}}{4}\frac{c_l^5}{\alpha_T^3}\,\Delta^2\left(\frac{3}{2}-\beta\right)^{-\frac{13}{2}}\right] * \left[\rho^2\,\tau_0^4\,\Omega^4\,k^{7/2}\exp\left(-\frac{\tau_0^2\,\Omega^2}{8}\right)\right] \tag{12}$$

More details about the method's functions like the modified convection factor Ω and the convective Mach number $M_c$, along with all its constants are available in previous works of [18] and [19]. In this forth-order correlation function (Eq.12), there is one calibration coefficient ($\alpha_T$) which need to be defined based on the experimental data.

Now, the acoustic field generated by the jet can be calculated, however, Eq. 11 and 12 doesn't account for any refraction effects caused by the velocity gradients in the flow. In order to incorporate this in the model, [19] uses the standard acoustic ray propagation equations by [24] and Blokhintzev [27] invariant definition to get to Eq. 13. This equation can calculate the sound pressure level variation due to the refraction effects.

$$\Delta SPL = 10 \log_{10} \left[ \frac{B_{source}}{B_{farfield}} \left[ \frac{N_{ray\ w/\ ref}}{N_{ray\ w/o\ ref}} \right]_{farfield} \right] \quad (13)$$

$$B = \frac{|V_{ray}|}{(1 - \overline{u_i}\, s_i)\overline{\rho}\, \overline{c}^2} \quad (14)$$

This equation evaluates the terms $V_{ray}$ and $s_i$, calculated from ray propagation equations, in both sound source and farfield locations. It also counts the number of rays $N_{ray}$ that crosses the same area in farfield with and without the refraction effect.

By calculating this Δ and summing the result with the sound pressure levels obtained from Eq. 11, the LRT method can calculate the SPL from a jet accounting for its refraction effect.

### 3.3 Geometry and Computational Mesh

The tridimensional domain was built with a block structured hexahedral mesh, refined in the nozzle's exit and along the jet's mixing layer (Fig. 8). The computational domain is $80D_j$ long and $40D_j$ wide from the jet's exit. The nozzle penetrates $1D_j$ in the domain and has a $8D_j$ length tube behind it. This setup is for reproducing closely the experimental conditions and maintaining the boundary condition as far as possible from the region of interest.

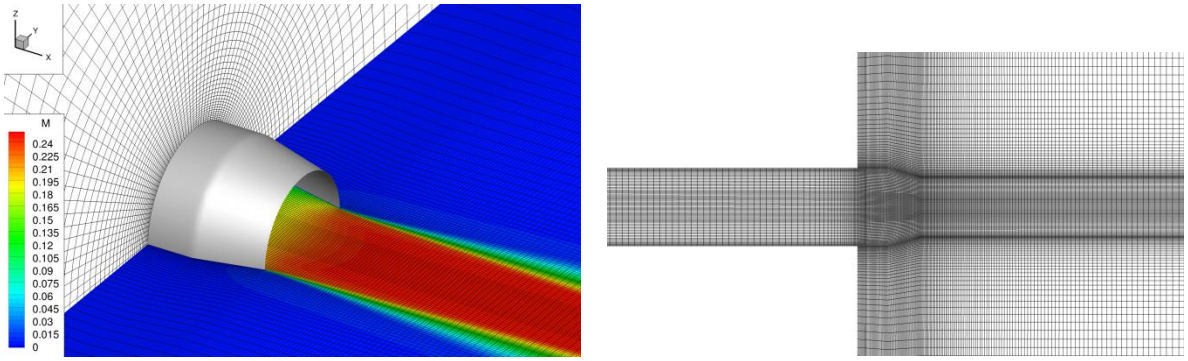


(a) Mesh refinement of the nozzle (b) Mesh detail in the nozzle region

Figure 8. Computational domain and mesh detail.

Various grid independency tests were made in order to get to the 2 million elements mesh used in this work.

### 3.4 Boundary Conditions and Setup

The conditions used by the simulations were the same measured in the experiments. The fluid is air, the ambient pressure and temperature were 101871 [Pa] and 291.23 [K] and the mean velocity measured at nozzle's exit was 85 [m/s]. The boundary conditions used were a viscous wall function for the jet's nozzle and tube, stagnation pressure and temperature set to 106397.931 [Pa] and 294.870 [K] at jet's inlet, simple back pressure imposition at outflow and Riemann invariants for the fairfield and domain's inflow.

### 3.5 Noise Prediction Parameters

The noise radiated from the jet encounters a quiescent flow in the farfield with pressure and temperature equals to the ambient. To run the ray tracing methodology, sound sources need to be placed into the flow field, and as expected, the positioning of these sources produces great effects in the final acoustics results. When using the ray tracing method in different problems, is recommended to place the sources in each mesh node in order to keep the precision from the earlier calculations. However this is unnecessary for a jet flow, as it is known from theory and experiments that the noise produced by this kind of flow is originated mostly in the jet's mixing layer. In fact, the noise generated by a jet flow originates from high turbulent kinetic energy zones spreading around the potential core from 0 up to 6 nozzle diameters in the streamwise direction.

By considering that, tracking an iso-surface of low turbulent kinetic energy delimitates a tridimensional region where the sound generation is important. Therefore if sound sources where distributed inside this region no errors will be carried in the further calculations. In this work, several tests where made with the sources number and positions, leading to use a tridimensional region delimited by 10% of the jet's maximum turbulent kinetic energy and $10^3$ sound sources distributed inside it.

## 4. Results

The results are split in two sub-sections, being firstly shown the aerodynamics characterization of the fluid flow by means of velocity profiles acquired by the Pitot tube and the single hot-wire anemometer. These results are seen in terms of the jet's centerline velocity, radial velocity profiles and the jet's wake characterization contours. The numerical results are confrontated against the experimental ones in order to validate the flow simulation by employing the k-ω SST model. The acoustic noise from experimental measurements and numerical results are presented in sequence by showing the sound pressure level spectra for different observer angles and the overall sound pressure level graph. The acoustic simulations were made aiming to validate the LRT method to describe the physics of the sound generation and propagation of this low-speed subsonic jet.

### 4.1 Aerodynamics Results

Results from hot-wire measurements for the normalized mean velocity from the jet's centerline, distributed along the jet axis domain, from 0 up to 13 diameters, at Mach number 0.25 and Reynolds number of $2{,}1 \times 10^5$ (based on the jet diameter and the jet velocity $U_j$), is shown in Fig. 9. The velocity is expected to be maximum and unchangeable until 4 to 5 diameters from the exit nozzle along the centerline, defining the potential core

length (Abramovich, 1963). As can be seen from Fig. 9, the potential core ends between 4 to 4.5 diameters downstream the jet axis.

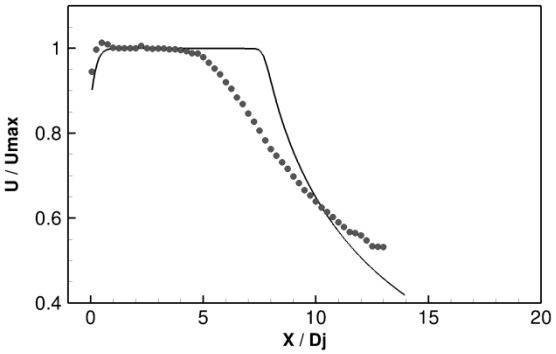


Figure 9. Velocity distribution along the jet axis. — CFD; ● Experiments (hot-wire).

On the other hand, the numerical model applied in the RANS calculation overpredicts the length of the core region, mainly due to the vortex-stretching and turbulence heterogeneity of the 3D flow-field not completely captured with RANS modelling. Although this trend is already expected by RANS calculations for axisymmetric jets, some turbulence models can enhance the prediction. In general the length of the potential core is over-predicted by numerical simulations in the range of 6 and 10 diameters, especially when considering standard $k-\varepsilon$ turbulence modelling [28], [29]. In addition to the wrong location of the potential core in Fig. 9, the rate of decay of the centreline axial velocity is also not fairly well approximated. Despite this well-known limitation of Reynolds average simulations, the results show a reasonable agreement to the experimental data when observing other fluid flow data.

In order to check the trend and the accuracy of the potential core length's prediction showed in Fig.9, the axial velocity centerline distribution has been obtained with hot-wire and Pitot tube. Additionally, the centerline for Mach condition M = 0.25 is also compared to other experimental reference from [10]. These comparisons can be seen in Fig. 10. It can be seen that at Mach number 0.25 the axial velocity profiles from the pitot and the hot-wire system are very similar. Far away around eleven diameters from the exit nozzle, the hot-wire results shown some inconsistency and it may be related to some unknown flow variation imposed by the compressor system during the measurement. The work of Morris and Zaman [10] shows only the results for Mach 0.25, alleging the fragility of the modern hot-wires probes with high frequency response to high and unsteady flows. Even though a slightly difference is seen in the size of the potential core (aproximatelly 6 diameters in reference [10]), the trend among the curves are consistent showing a similar rate decay. As stated before, the measurements performed in this work for the length of the potential core are within the experimental range cited in classical literature.

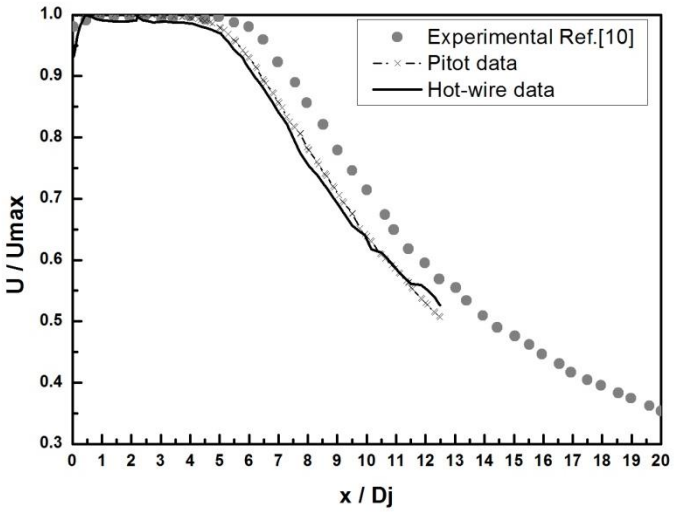


Figure 10. Velocity distribution along the jet axis for centerline at Mach 0.25. — Hot-wire; - - Pitot tube; Δ Morris and Zaman [10].

Despite a difference between the numerical and experimental results for the velocity distribution along the jet axis, a better agreement is shown for the radial velocity according to Fig. 10. Here, the experimental data where mirrored by the centerline to well characterize the jet's wake at streamwise locations of x/D = 0.0, 1.0, 2.0, 3.0, 4.0 and 5.0. Inside the potential core region, less than 5 nozzle diameters, the numerical results fit well against the experimental data. For x/D = 0.0 and 1.0, some discrepancies can be noticed, essentially related to the preditions having smother profiles due to the boundary conditions imposed to the flow.

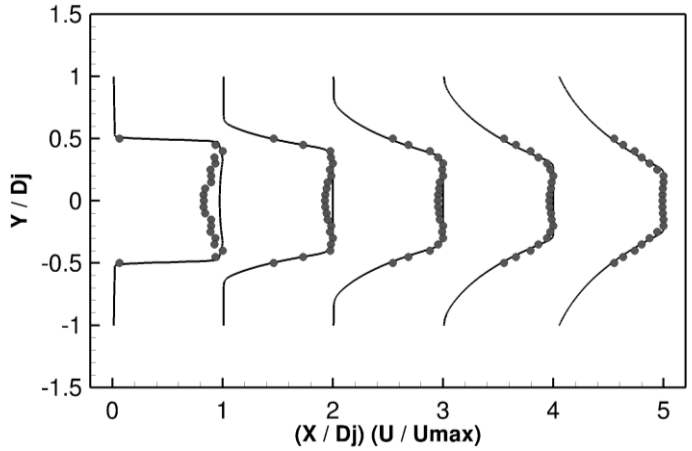


Figure 11. Velocity distribution along the jet radius. — CFD; ● Experiments (hot-wire).

To explore the flow field of this single jet, a wake flow characterization has been considered by its velocity distribution (contours). Since the whole experiment covered 963 points from Pitot tube and 593 points for hot-wire probes, it was possible to create the mean velocity contours. Thus, all lines measured are considered and, such as in the previous sub-section, the data is mirrored along the jet centerline to better characterize the wake. Although it seems to be merely illustrative or qualitative, it helps to summarize the information given from the velocity profiles. Figure 12 (a) shows the experimental mean velocity distribution from the exit nozzle to

thirteen diameters downstream the jet axis, also covering two diameters from the center of the nozzle. In Fig. 12 (b) the numerical results are presented where it is possible to see the potential core and the shear layer pattern. As mentioned before, the RANS simulation is not able to predict the length of the potential core and slight difference is also shown in the shear layer spreading. These discrepancies are important to be considered and is expected to have some influence in the noise predictions, since the LRT model is based on the primitive variables (*u*, *v*, *w*) and turbulence quantities (k, ω) of the fluid flow.

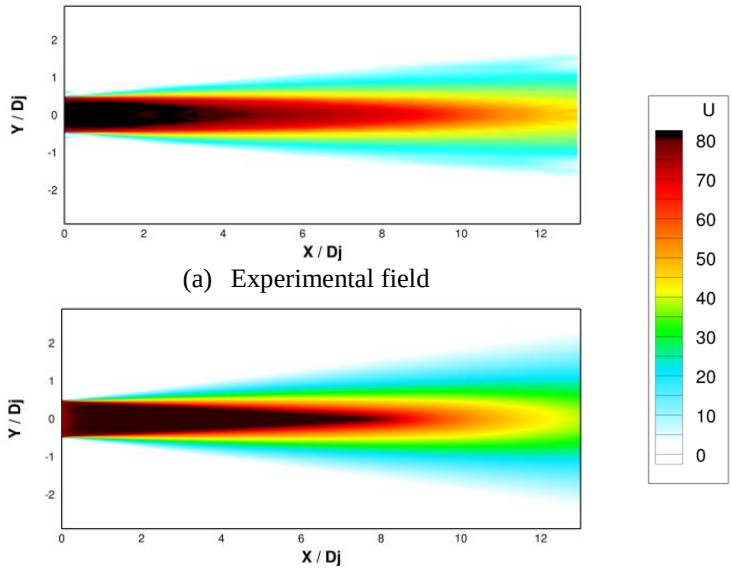


(a) Experimental field

(b) RANS simulation

Figure 12. Jet's wake velocity contours with Pitot tube data and CFD simulation, for Mach 0.25.

Figure 13 shows the jet's wake velocity contours obtained with hot-wire data. As stated earlier, the survey points region for the hot-wire sensor is smaller, only 593 points inside the potential core region. Thus, the shear layer is not entirely seen as shown in Figure 12(a). However, the results are very consistent and allow a good description of the jet's wake.

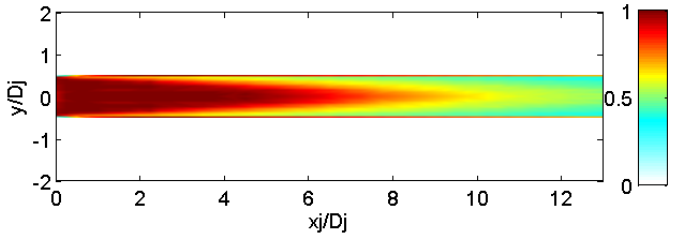


Figure 13. Jet's wake velocity contours with hot-wire data, for Mach 0.25.

Centerline variation of axial turbulence intensity is given in Figure 14. It is known that for application of single wire for measuring fluctuations, a reliable range to the sensor is around 10 up to 15% of the mean value. In this case, it can be seen that the peak turbulence intensity reaches aproximatelly 14% at x/Dj = 9,5 downstream. This result is consistent with other experimental measurents available such as the work of Morris

and Zaman (2010). It is also known that along the shear layer of a subsonic jet, the maximum values of turbulence intensity is around 15%. In Fig. 14 it is clear that the RANS calculation under-predicts the peak location and intensity. It is important to emphasize that the turbulence model coefficients have not been optimized for the studied case, assuming the standard values as seen in Table 1.

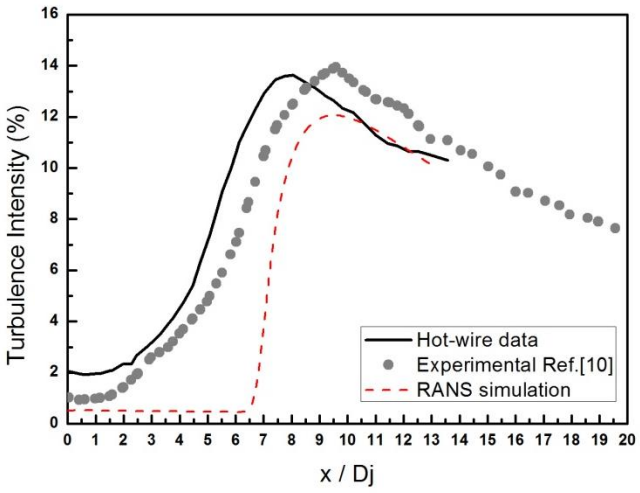


Figure 14. Turbulence intensity along the jet axis for centerline at Mach 0.25. — Hot-wire; ● Morris and Zaman (2010), - - - RANS simulation.

**4.2 Aeroacoustics Results**

The fluid flow predictions obtained with the RANS simulations were used as input information for the LRT method. Results of sound pressure spectra are presented for observer angles varying from 40º to 110º, as shown in Figure 15. During the acoustic measurements the arc of microphones was positioned at approximately 100 Dj from the nozzle exit and the noise data are corrected for a lossless condition at 1 m. The results are presented in terms of 1/3-octave band spectra. Figure 15 shows the comparison between the experimental and numerical data for all angles proposed. Acoording to the fluid flow and acoustics the sound sources are convected downstream by the mean flow and the maximum noise is radiated and expected to happen at observer angles between 30° and 50°, making its directivity evidentiated.

By inspecting the sound pressure spectra in Fig. 15 the most significant difference between the numerical predictions and experimental data is found for 40° angle. Even though the RANS simulations showed discrepancies for the fluid flow, it is possible to affirm that the LRT method was capable to predict the sound spectra with an acceptable level of agreement for all the angles investigated. However, at smaller (shallow) angles such as 40º and 50º the LRT starts to loose its precision since there is a very large noise attenuation (zone of silence) due to the refraction effects caused by the fluid flow – these effects have been shown in

literature [2], [19], [30] among others. Despite such discrepancy at this angle, it is important to state that this difference is not over 2 dB.

In Fig. 15 (e) the peak noise is predicted fairly well by the LRT method, despite the fact that the peak noise is strongly related to the end of the potential core. As seen before, there is a mismatch between the fluid flow prediction and the experimental data for the length of the potential core. In this case, such discrepancy was not considerable to change the peak noise level.

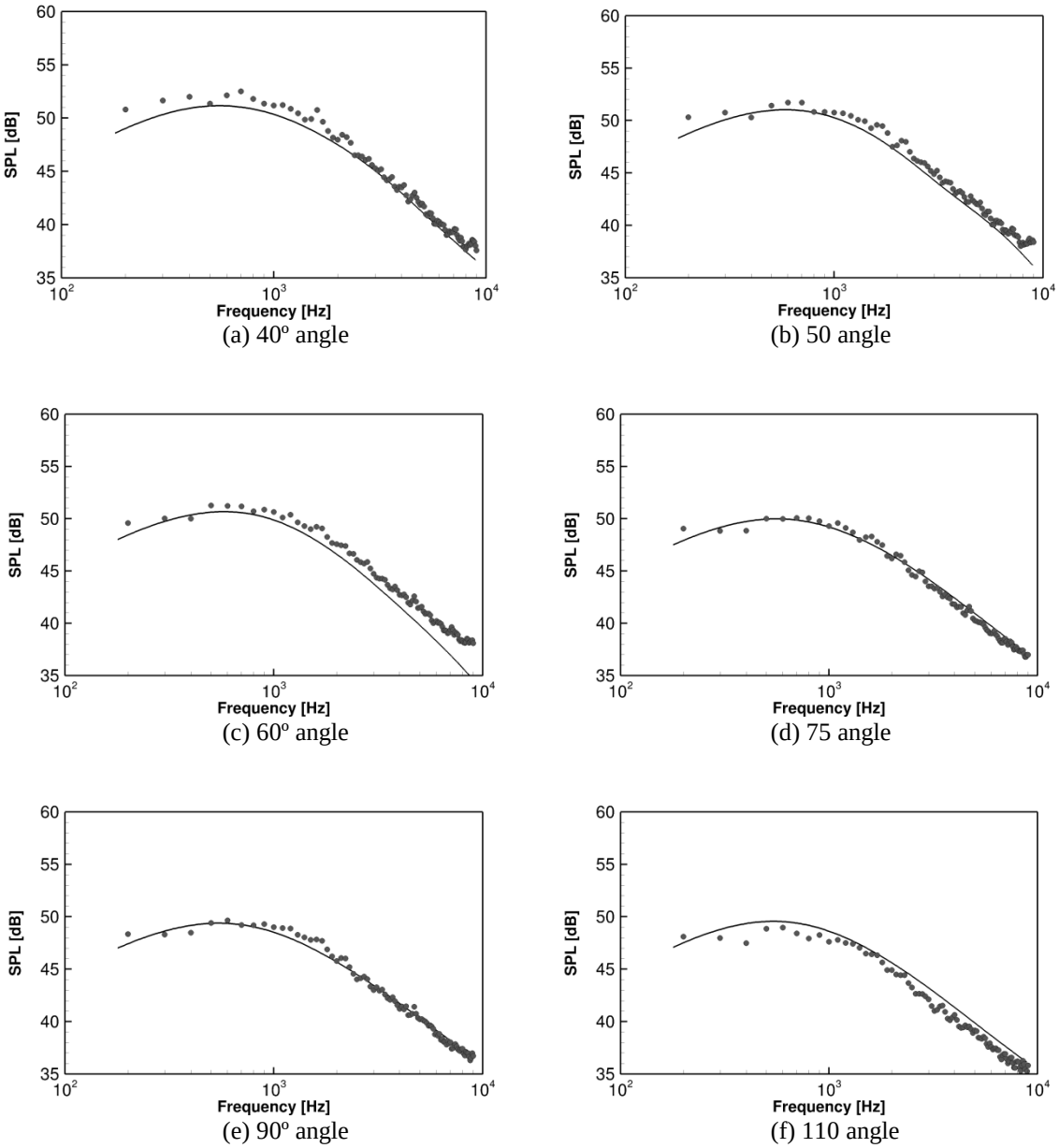


(a) 40º angle (b) 50 angle

(c) 60º angle (d) 75 angle

(e) 90º angle (f) 110 angle

Figure 15. Sound Pressure Level Spectra for Mach number 0.25 single jet for angles varying from 40 up to 110º. — LRT; ● Experiments.

Finally, Fig. 16 shows the overall sound pressure level (OASPL), by comparing the LRT results with the experimental data. It is possible to see that the LRT method can be used to quantify the acoustic noise of single stream jet flows with reasonable accuracy and relatively low computational cost. In terms of overall SPL, the difference of 2 dB, as stated before, at 40° is better noticed in Fig. 16.

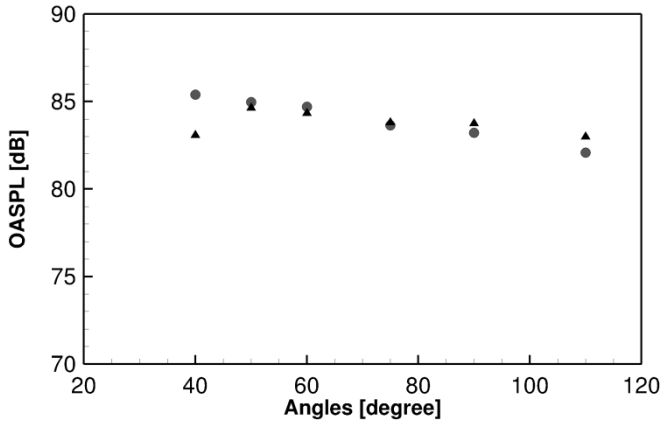


Figure 16. Overall Sound Pressure Level for Mach number 0.25 single jet for angles varying from 40 up to 110º. ▲ LRT; ● Experiments

## 5. Conclusions

This paper has described aerodynamics and aeroacoustics characterization of a low-speed subsonic jet operating at Mach 0.25 through experimental and numerical techniques. The main goal was to couple experimental and numerical tools to fundamentally study this kind of flow pattern. The experimental data gathered with Pitot tube and hot-wire anemometer was used as an original benchmark for the validation of a RANS-based method coupled with an acoustic noise modeling (LRT method) to predict the noise at specific locations in the farfield, providing a relatively low-cost methodology that could be applied in the aeronautical context. The results were discussed sequentially from the aerodynamics experimental and numerical data, which compounds most of the efforts in terms of experiments, post-processing and analyses. Additionaly, some experimental results are also compared with other data available from literature identifying some possible drawbacks in such kind of measurements. Deviations were observed in the fluid flow predictions and are purely related to the RANS approach considered. The acoustic results are shown to six observer positions in the farfield. The experimental data is confronted to the numerical RANS-based method coupled with the LRT method, showing a very good agreement even for shallow angles. The numerical results for the acoustic and flow fields were well compared with the experimental data, showing that this low-cost flow-acoustic methodology can be used to predict acoustic noise of subsonic jet flows, even at low speeds.

## Acknowledgments

The study reported herein was partially funded by EMBRAER and FAPESP under the GRANT Nº 06/52568-7 The authors also would like to thank the financial support provided by Coordenação de Aperfeiçoamento de Pessoal de Ensino Superior (CAPES) and the Fundação de Amparo à Pesquisa do Estado de Minas Gerais (FAPEMIG). The first author gratefully acknowledge the support received at the Institute of Sound and Vibration for the conclusion of his MsC thesis. The second author also thanks the collaboration between the Institute of Sound and Vibration Research (ISVR) – United Kingdom and the Faculty of Mechanical Engineering at Federal University of Uberlândia (UFU) – Brazil.

## References

[1] Smith, M., *Aircraft Noise*. Cambridge aerospace series, 3, Cambridge University Press, Cambridge, New York, (1989).

[2] Almeida, O., Aeroacoustics of Dual-stream Jets with Application to Turbofan Engines, Thesis of Doctor of Science − Aeronautics Institute of Technology, São José dos Campos, (2009).

[3] Federal Aviation Administration, *Code of Federal Regulations. Part 36: noise standards: aircraft type and airworthiness certification*, Washington, DC., Jul. (2002), (Final Rule Docket n. FAA-2000-7587).

[4] TrüPel, T., Über die Einwirkung eines Luftstrahles auf die umgebende Luft. München, Oldenbourg, (1914).

[5] Abramovich, G. N., *The Theory of Turbulent Jets*, Edited by Leon H. Schindel, The MIT Press Classics, (1963).

[6] Townsend, A. A., *The Structure of Turbulent Shear Flow*, Cambridge University, (1956).

[7] Lilley, G. M., On the noise from air jets. Aero. Res. Counc., Lond., **20**,376-N. 40- F.M. 2724, (1958).

[8] Lau, J.C. and Tester, B.J., An Evaluation of the Lighthill Analogy for Jet Mixing Noise Generation: Using LV Turbulence, Source Location and Spectral Noise Data, *IUTAM/ICA/AIAA-Symposium Gottengen*, (1979).

[9] Harper-Bourne, M., Jet noise turbulence measurements, 9*th AIAA/CEAS Aeroacoustics Conference and Exhibit*, 12-14 May (2003).

[10] Morris, P. J. and Zaman, K.B.M.Q., Velocity measurements in jets with application to noisesource modeling, *Journal of Sound and Vibration*, 329, pp. 394–414, (2010).

[11] Mielke, A. F., Seasholtz, R. G., Elam, K. A. and Panda, J., Time-average molecular Rayleigh scattering technique for measurement of velocity, density, temperature, and turbulence intensity in high speed nozzle flows, *AIAA-2004-0706*, (2004).

[12] Bridges, J., Wernet, M. P. and Brown, C., Control of jet noise through mixing enhancement, NASA TM-2003-212335, (2003).

[13] Ghahremanian, S. and Moshfegh, B., Numerical and experimental verification of initial, transitional and turbulent regions of free turbulent round jet, *20th AIAA Computational Fluid Dynamics Conference*, 27-30 June, Honolulu, Hawaii, (2011).

[14] Freund J. B., Noise sources in a low-Reynolds-number turbulent jet at Mach 0.9, *J. Fluid Mech*, **438**:277–305, (2001).

[15] Stromberg J. L., McLaughlin D. K. and Troutt T. R., Flow field and acoustic properties of a Mach number 0.9 jet at a low Reynolds number, *J Sound Vib*, **72**:159–76, (1980).

[16] Xia H., Tucker P. G. and Eastwood S., Large-eddy simulations of chevron jet flows with noise predictions, *Int J Heat Fluid Flow*, **30**:1067–79, (2009).

[17] Birch S. F., Lyubimov D. A. and Maslov V. P., Secundov AN. Noise prediction chevron nozzle, In: *12th AIAA/CEAS* conf. p. 2600, (2006).

[18] Engel R.C., Silva, C.R.I. and Deschamps, C. J., Application of RANS-based method to predict acoustic noise of chevron nozzles, *Applied Acoustics*, **79** 153-163, (2014).

[19] Silva C.R.I., Desenvolvimento de um novo método RANS-based para a aeroacústica computacional de jatos de alta velocidade, Thesis (Ph.D. thesis in Mechanical Engineering). University of São Paulo, São Paulo; (2011).

[20] Proença, A.R., Experimental characterization of velocity and acoustic fields of single-stream subsonic jet, Thesis (MsC thesis in Mechanical Engineering). University of Uberlândia, Uberlândia, (2013).

[21] Pinker, R.A, The Enhancement of the QinetiQ Noise Test Facility for Larger Scale Exhaust Systems, *AIAA-2004-3019*, (2004).

[22] Metacomp Technologies INC. *User's manual*, (2009).

[23] Menter, F. R., Zonal two equation k-ω turbulence models for aerodynamic flows, *AIAA* Paper **93-**2906, (1993).

[24] Pierce, A. D., *Acoustics: An Introduction to Its Physical Principles and Applications*, McGraw-Hill, New York, (1981).

[25] Khavaran, A., Krejsa, E. A. and Kim, C. M., Computation of supersonic jet mixing noise for an axisymmetric cd nozzle using k-ε turbulence model, NASA, TM 105338, (1992).

[26] Jordan, P. and Gervais, Y., Modeling self- and shear-noise mechanisms in inhomogeneous, anisotropic turbulence, *Journal of Sound and Vibration*, vol. **279**, pp. 529-555, (2005).

[27] Blokhintzev, D., The propagation of sound in an inhomogeneous and moving medium, *The Journal of the Acoustical Society of America*, Vol. **18**(2), pp. 322–328, (1945).

[28] Birch SF, Bukshtab PA, Khritov KM, Lyubimov DA, Maslov VP, Secundov AN, Yakubovsky K Ya. A RANS based jet noise prediction procedure, In: *13th AIAA/CEAS* conf.; p. 3727, (2007).

[29] Engblom WA, Khavaran A, Bridges J., Numerical prediction of chevron nozzle noise reduction using WIND-MGBK methodology. In: *10th AIAA/CEAS* conf.;. p. 2979, (2004).

[30] Balsa, T.F., Gliebe, P.R., Kantola, R.A, Wang, J.C.F, Mani, R., High Velocity Jet Noise Source Location and Reduction: Task 2 – Theoretical Developments and Basic Experiments, Washington-DC: Federal Aviation Administration Report, FAA-RD-76-79-II, 1978.